AFRL-RX-WP-JA-2018-0101

SURFACE PLASMON ABSORPTION IN MoS_2 AND GRAPHENE-MoS_2 MICRO-GRATINGS AND THE IMPACT OF A LIQUID CRYSTAL SUBSTRATE (POSTPRINT)

V. Yu. Reshetnyak, V. I. Zadorozhnii, and I. P. Pinkevych

Taras Shevchenko National University of Kyiv

T. J. Bunning and D. R. Evans

AFRL/RX

15 FEBRUARY 2018
Interim Report

AIR FORCE RESEARCH LABORATORY
MATERIALS AND MANUFACTURING DIRECTORATE
WRIGHT-PATTERSON AIR FORCE BASE, OH 45433-7750
AIR FORCE MATERIEL COMMAND
UNITED STATES AIR FORCE

REPORT DOCUMENTATION PAGE

Form Approved
OMB No. 0704-0188

1. REPORT DATE *(DD-MM-YY)*	2. REPORT TYPE	3. DATES COVERED *(From - To)*
15 February 2018	Interim	23 August 2016 – 15 January 2018

4. TITLE AND SUBTITLE
SURFACE PLASMON ABSORPTION IN MoS2 AND GRAPHENE-MoS2 MICRO-GRATINGS AND THE IMPACT OF A LIQUID CRYSTAL SUBSTRATE (POSTPRINT)

5a. CONTRACT NUMBER
FA8650-16-F-5419

5b. GRANT NUMBER

5c. PROGRAM ELEMENT NUMBER
62102F

6. AUTHOR(S)
1) V. Yu. Reshetnyak, V. I. Zadorozhnii, and I. P. Pinkevych – TSNU
2) T. J. Bunning and D. R. Evans – AFRL/RX

5d. PROJECT NUMBER
4348

5e. TASK NUMBER

5f. WORK UNIT NUMBER
X14W

7. PERFORMING ORGANIZATION NAME(S) AND ADDRESS(ES)
1) Taras Shevchenko National University of Kyiv
Kyiv 01601, Ukraine
2) AFRL/RX
Wright-Patterson AFB
Dayton, OH 45433

8. PERFORMING ORGANIZATION REPORT NUMBER

9. SPONSORING/MONITORING AGENCY NAME(S) AND ADDRESS(ES)
Air Force Research Laboratory
Materials and Manufacturing Directorate
Wright-Patterson Air Force Base, OH 45433-7750
Air Force Materiel Command
United States Air Force

10. SPONSORING/MONITORING AGENCY ACRONYM(S)
AFRL/RXAP

11. SPONSORING/MONITORING AGENCY REPORT NUMBER(S)
AFRL-RX-WP-JA-2018-0101

12. DISTRIBUTION/AVAILABILITY STATEMENT
Distribution Statement A. Approved for public release: distribution unlimited.

13. SUPPLEMENTARY NOTES
PA Case Number: 88ABW-2018-0731; Clearance Date: 15 Feb 2018. This document contains color. Journal article published in AIP Advances, Vol. 8, No. 4, 27 Apr 2018. © 2018Author(s) The U.S. Government is joint author of the work and has the right to use, modify, reproduce, release, perform, display, or disclose the work.
The final publication is available at https://doi.org/10.1063/1.5032297

14. ABSTRACT *(Maximum 200 words)*
The absorption coefficients of a far-infrared wave are calculated at normal incidence for MoS_2 and graphene-MoS_2 micro-ribbon gratings placed between a nematic LC and an isotropic dielectric medium. Maxima in the absorption spectra, which are related to the excitation of the surface plasmons in micro-ribbons of these gratings, are observed. The spectral position of absorption maxima depends on the grating spacing, micro-ribbon width, and conductivity of the ribbons. The impact of the 2D electron concentration of the MoS_2 ribbons on the plasmon bands is different for a MoS_2-grating versus a graphene-MoS_2 grating. The influence of the LC orientational state on the absorption spectra of the gratings enables the manipulation of the absorption peak magnitude.

15. SUBJECT TERMS
absorption coefficients; far-infrared wave; MoS_2; graphene-MoS_2; micro-ribbon grating; nematic LC; isotropic dielectric

16. SECURITY CLASSIFICATION OF:			17. LIMITATION OF ABSTRACT:	18. NUMBER OF PAGES	19a. NAME OF RESPONSIBLE PERSON (Monitor)
a. REPORT	b. ABSTRACT	c. THIS PAGE			Timothy White
Unclassified	Unclassified	Unclassified	SAR	12	19b. TELEPHONE NUMBER *(Include Area Code)* (937) 255-9551

Surface plasmon absorption in MoS_2 and graphene-MoS_2 micro-gratings and the impact of a liquid crystal substrate

V. Yu. Reshetnyak,[1] V. I. Zadorozhnii,[1,a] I. P. Pinkevych,[1] T. J. Bunning,[2] and D. R. Evans[2]

[1]*Physics Faculty, Taras Shevchenko National University of Kyiv, Kyiv 01601, Ukraine*
[2]*Air Force Research Laboratory, Materials and Manufacturing Directorate, Wright-Patterson Air Force Base, OH 45433, USA*

(Received 4 April 2018; accepted 16 April 2018; published online 27 April 2018)

The absorption coefficients of a far-infrared wave are calculated at normal incidence for MoS_2 and graphene-MoS_2 micro-ribbon gratings placed between a nematic LC and an isotropic dielectric medium. Maxima in the absorption spectra, which are related to the excitation of the surface plasmons in micro-ribbons of these gratings, are observed. The spectral position of absorption maxima depends on the grating spacing, micro-ribbon width, and conductivity of the ribbons. The impact of the 2D electron concentration of the MoS_2 ribbons on the plasmon bands is different for a MoS_2-grating versus a graphene-MoS_2 grating. The influence of the LC orientational state on the absorption spectra of the gratings enables the manipulation of the absorption peak magnitude. https://doi.org/10.1063/1.5032297

I. INTRODUCTION

A possible way to control terahertz (THz) radiation is based on using micro-ribbon gratings.[1] In the mid-infrared and far-infrared (THz) spectral region, electromagnetic radiation cannot couple to plasmon excitations in metallic or semiconductor sheets due to the large wave vector mismatch between the plasmonic and incident electromagnetic waves.[2] However, plasmons can be excited in the gratings comprised of metallic or semiconductor ribbons with dimensions much smaller than the radiation wavelength. In such gratings, plasmons can be controlled by manipulation of the micro-ribbon width or the grating spacing.

Surface plasmons at terahertz frequencies in grating structures with ribbons were first excited in graphene micro-ribbons and in graphene nano-ribbons on different supporting substrates.[1,3–6] It allowed developing various devices, in particular tunable absorbers[7–9] and polarizers.[10] The operating frequency of a large number of optoelectronic devices extends from the infrared to the THz spectral range and, therefore, study of the THz dielectric response in materials is very important.[11–14] The resonant plasmon frequency in grating structures depends on the dielectric properties of the layers neighboring with the grating. By adjusting the permittivity of the grating substrates or the Fermi energy of the grating ribbons, it is possible to change the optical properties of the grating based devices.[15–17] A liquid crystal (LC) can also be used as the dielectric substrate of the grating.[18] The LC permittivity is anisotropic and depends on the LC director. It can be changed by applying electric and magnetic fields or other external stimuli.[19]

In addition to the graphene, a monolayer molybdenum disulphide (MoS_2) is also very perspective plasmonic material possessing high field confinement and low losses.[20] MoS_2 was recently proposed for exciting surface plasmons in the mid-infrared and far-infrared spectral region.[21]

[a]Corresponding author e-mail address: v.i.zador@gmail.com

The presence of a bandgap in a MoS_2 monolayer allows the fabrication of transistors that can be turned off and used as switches, logic circuits, and high gain amplifiers.[22] Electro-optic modulators, photodetectors, optical filters, and phase shifters can also be developed using a MoS_2 monolayer.[21,23,24] Recently, different MoS_2/graphene hybrid heterostructures have been demonstrated. In particular, the appearance of hexagonal flakes at the chemical vapor deposition of MoS_2 on a graphene surface,[25] formation of the van der Waals heterostructures in a growth process of the MoS_2 on epitaxial graphene,[26] the chemically assembled atomic sized transistors based on single-layer MoS_2 and graphene heterostructures,[27] parallel stitched MoS_2-graphene heterostructures as a prototype of metal–semiconductor heterostructures.[28]

In the present paper, we study the light absorption in MoS_2 and graphene-MoS_2 micro-ribbon gratings. We propose to place a LC slab near the gratings and study the possibility of controlling the absorption of these structures in the THz range by reorienting the LC director with an applied field.

The paper is organized as follows. In Sec. II we introduce a model of the LC-grating-dielectric structure and present equations allowing for the calculation of the absorption coefficient for the system. Results of numerical calculations of the absorption coefficient in MoS_2 and graphene-MoS_2 micro-ribbon gratings and their discussion are presented in Sec. III. In Sec. IV we present some brief conclusions.

II. MODEL AND EQUATIONS FOR THE LIGHT FIELD

Let a micro-grating located in the xy-plane is placed between a nematic LC layer (top substrate) and an isotropic dielectric substrate (Fig. 1). The grating is comprised of single layer ribbons made from two different metals (or semi-metals). The ribbons are directed along the y-axis; d and Λ - d are the widths of the adjacent ribbons, Λ is the grating spacing. A plane electromagnetic wave falls on the grating from the side of the LC and excites the surface plasmon polaritons (SPPs) in the grating ribbons. In order to excite the SPPs the light wave electric vector must have the component directed along the grating perpendicular to its ribbons. We consider a normal incidence of the light wave on the grating. Therefore, we can set the magnetic vector of the incident wave to be directed along the y-axis (TM-wave). To avoid the complicated factors at the calculations we assume: i) the system to be infinite in the y-direction; ii) the substrates are semi-infinite in the z-direction; iii) the LC director is located in the xz-plane.

The SPPs are strongly localized near the ribbons, therefore only the thin layer of the LC adjacent to the ribbons can influence the SPPs. To simplify calculations we set the LC director profile in the whole substrate to be the same as in the layer near the ribbons. It allows considering the LC substrate as a homogeneous anisotropic medium.

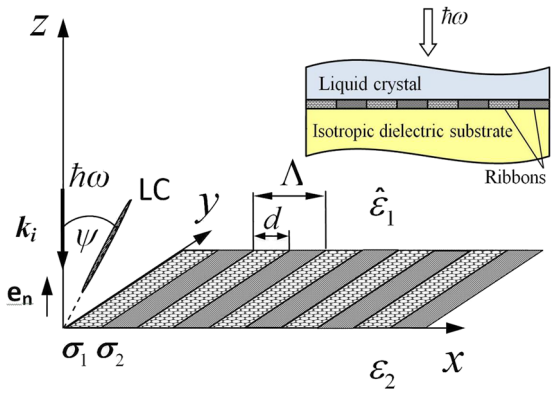

FIG. 1. Experimental set-up, showing the TM-wave with the wave vector $\boldsymbol{k}_i$ incident from the LC on the grating-dielectric structure. Λ is the grating spacing, d, $\Lambda - d$ and σ_1, σ_2 are the widths and the conductivity of the ribbons, respectively; $\hat{\varepsilon}_1$ is the LC dielectric tensor, ε_2 is the isotropic substrate permittivity, ψ is the director orientation angle in the xz-plane, $\mathbf{e_n}$ is a normal to the ribbons plane.

As the TM-wave in the LC is normally incident on the grating, the electric and magnetic vectors of this wave can be written in the form:

$$\mathbf{E}_{\mathrm{i}} = (E_{ix}\mathbf{e}_x + E_{iz}\mathbf{e}_z)\ \mathrm{e}^{-i\,(k_i\,z+\omega\,t)}, \quad \mathbf{H}_i = H_i\ e^{-i\ (k_i\,z+\omega\,t)}\mathbf{e}_y. \tag{1}$$

Satisfying the Maxwell equations, we obtain that

$$E_{iz} = -(\varepsilon_{1xz}/\varepsilon_{1zz})\ E_{ix}, \quad H_i = -\frac{k_i}{\omega\,\mu_0}E_{ix} \tag{2}$$

and the wave vector is determined by the dispersion equation

$$k_i = \frac{\omega}{c}\sqrt{\varepsilon_{1xx} - \frac{{\varepsilon_{1xz}}^2}{\varepsilon_{1zz}}} \tag{3}$$

with ε_{1ij} denoting the LC dielectric tensor component.

The system is periodic along the x-axis and for reflected and transmitted waves we can use the Fourier-Floquet expansion. Then, the electric and magnetic vectors of the reflected wave, which satisfy the Maxwell equations in the LC are as follows (see Ref. 18):

$$\begin{aligned}
\mathbf{E}_r &= \frac{c/\left(\omega\,\varepsilon_{1zz}\right)}{\sqrt{\varepsilon_{1xx} - \frac{{\varepsilon_{1xz}}^2}{\varepsilon_{1zz}}}}\ \sum_n \left[\left(\varepsilon_{1zz}k_{rn} + \varepsilon_{1xz}k_n\right)\ \mathbf{e}_x - \left(\varepsilon_{1xz}k_{rn} + \varepsilon_{1xx}k_n\right)\mathbf{e}_z\right]\ a_n\ e^{i\ (k_n\,x+k_{rn}\,z-\omega\,t)}, \\
\mathbf{H}_r &= \varepsilon_0\,c\sqrt{\varepsilon_{1xx} - \frac{{\varepsilon_{1xz}}^2}{\varepsilon_{1zz}}}\ \sum_n a_n\ e^{i\ (k_n\,x+k_{rn}\,z-\omega\,t)}\ \mathbf{e}_y.
\end{aligned} \tag{4}$$

The corresponding dispersion equation takes the following form:

$$k_{rn} = \sqrt{\left(\varepsilon_{1xx} - \frac{{\varepsilon_{1xz}}^2}{\varepsilon_{1zz}}\right)}\sqrt{\left(\frac{\omega^2}{c^2} - \frac{{k_n}^2}{\varepsilon_{1zz}}\right)} - \frac{\varepsilon_{1xz}}{\varepsilon_{1zz}}k_n. \tag{5}$$

For the transmitted wave in the isotropic dielectric substrate we obtain

$$\begin{aligned}
\mathbf{E}_t &= -\frac{c}{\omega\sqrt{\varepsilon_2}}\sum_n \left(k_{t\,n}\mathbf{e}_x + k_n\mathbf{e}_z\right)\ b_n\ e^{i\ (k_n\,x-k_{tn}\,z-\omega\,t)}, \\
\mathbf{H}_t &= \varepsilon_0\,c\sqrt{\varepsilon_2}\ \sum_n b_n\ e^{i\ (k_n\,x-k_{tn}\,z-\omega\,t)}\mathbf{e}_y
\end{aligned} \tag{6}$$

and the dispersion equation

$$k_{t\,n} = \sqrt{\frac{\omega^2}{c^2}\varepsilon_2 - {k_n}^2}. \tag{7}$$

Here a_n, b_n are the coefficients of the Fourier-Floquet expansions for reflected and transmitted waves, respectively; $k_n = 2\pi n/\Lambda$, n is the number of the Fourier-Floquet spatial harmonic, ε_2 is the isotropic substrate dielectric permittivity.

The electric and magnetic vectors of the incident, reflected, and transmitted waves satisfy the boundary conditions at the grating ($z = 0$):

$$\begin{aligned}
\left[\mathbf{e_n} \times \left(\mathbf{H}_i + \mathbf{H}_r - \mathbf{H}_t\right) - \mathbf{j}_s\right]|_{z=0}\ \mathbf{e}_x = 0, \\
\left[\mathbf{e_n} \times \left(\mathbf{E}_i + \mathbf{E}_r - \mathbf{E}_t\right)\right]|_{z=0}\ \mathbf{e}_y = 0,
\end{aligned} \tag{8}$$

where $\mathbf{j}_s = \sigma(x)E_{tx}(z=0)\ \mathbf{e}_x$ is a current density in the plane of the grating with $\sigma(x)$ to be the grating surface conductivity. Using expression for $E_{tx}(z=0)$ from Eq. (6), we get

$$\mathbf{j}_s = -\sigma(x)\,\frac{c}{\omega\sqrt{\varepsilon_2}}\ \sum_n k_{t\,n}b_n\ e^{i\ (k_n\,x-\omega\,t)}\ \mathbf{e}_x\,. \tag{9}$$

Substitution of Eqs. (9) and (1)–(7) for electric and magnetic vectors into the boundary conditions (8) yields the following equations for coefficients a_n, b_n:

$$\sum_n \left[\sqrt{\varepsilon_{1xx} - \frac{{\varepsilon_{1xz}}^2}{\varepsilon_{1zz}}}\, a_n - \left(\sqrt{\varepsilon_2} + \sqrt{\frac{\omega^2}{c^2} - \frac{4\pi^2 n^2}{\varepsilon_2 \Lambda^2}}\, \frac{\sigma(x)}{\varepsilon_0 \omega} \right) b_n \right] e^{\frac{2i\pi nx}{\Lambda}} - \sqrt{\varepsilon_{1xx} - \frac{{\varepsilon_{1xz}}^2}{\varepsilon_{1zz}}}\, E_{ix} = 0\,, \tag{10}$$

$$\sum_n \left[\sqrt{\frac{\omega^2}{c^2} - \frac{4\pi^2 n^2}{\varepsilon_{1zz}\Lambda^2}}\, a_n + \sqrt{\frac{\omega^2}{c^2} - \frac{4\pi^2 n^2}{\varepsilon_2 \Lambda^2}}\, b_n \right] e^{\frac{2i\pi nx}{\Lambda}} + \frac{\omega}{c} E_{ix} = 0\,. \tag{11}$$

Eqs. (10) and (11) were obtained before in our previous paper[18] in the case of the graphene grating. Here we use these equations for the case of the more complicated grating comprised of the micro-ribbons made from two different materials.

We represent a function $\sigma(x)$ in Eq. (10) in the form of a step function

$$\sigma(x) = \begin{cases} \sigma_1, & n\Lambda < x < n\Lambda + d \\ (\sigma_1 + \sigma_2)/2, & x = n\Lambda + d \\ \sigma_2, & n\Lambda + d < x < (n+1)\Lambda \end{cases}, \tag{12}$$

where σ_1 and σ_2 are the surface conductivities of the adjacent ribbons (see Fig. 1).

Using Eq. (12) and performing some algebra we arrive at the following equations for coefficients a_n, b_n:

$$\left[\sqrt{\frac{\omega^2}{c^2} - \frac{4\pi^2 n^2}{\varepsilon_{1zz}\Lambda^2}} \left(\frac{\sigma_1 d + \sigma_2 (\Lambda - d)}{\varepsilon_0 \omega\, \Lambda} + \frac{\sqrt{\varepsilon_2}}{\sqrt{\frac{\omega^2}{c^2} - \frac{4\pi^2 n^2}{\varepsilon_2 \Lambda^2}}} \right) + \sqrt{\varepsilon_{1xx} - \frac{{\varepsilon_{1xz}}^2}{\varepsilon_{1zz}}} \right] a_n + \sum_{m(m\neq n)} \frac{i(\sigma_1 - \sigma_2)\left(e^{\frac{2i\pi(m-n)d}{\Lambda}} - 1\right) \sqrt{\frac{\omega^2}{c^2} - \frac{4\pi^2 m^2}{\varepsilon_{1zz}\Lambda^2}}}{2\pi\omega\varepsilon_0 (n-m)}\, a_m \tag{13}$$

$$= \left[\sqrt{\varepsilon_{1xx} - \frac{{\varepsilon_{1xz}}^2}{\varepsilon_{1zz}}} - \frac{\sigma_1 d + \sigma_2 (\Lambda - d)}{\varepsilon_0 c \Lambda} - \frac{\sqrt{\varepsilon_2}\,\omega/c}{\sqrt{\frac{\omega^2}{c^2} - \frac{4\pi^2 n^2}{\varepsilon_2 \Lambda^2}}} \right] E_{ix}\delta_{n0} - \frac{i(\sigma_1 - \sigma_2)\left(e^{\frac{-2i\pi n d}{\Lambda}} - 1\right)}{2\pi\varepsilon_0 n c} E_{ix}(1 - \delta_{n0}),$$

$$b_n = -\frac{1}{\sqrt{\frac{\omega^2}{c^2} - \frac{4\pi^2 n^2}{\varepsilon_2 \Lambda^2}}} \left(\frac{\omega}{c} E_{ix}\delta_{n0} + \sqrt{\frac{\omega^2}{c^2} - \frac{4\pi^2 n^2}{\varepsilon_{1zz}\Lambda^2}}\, a_n \right). \tag{14}$$

Numerically solving Eqs. (13) and (14) we can calculate coefficients a_n, b_n and the electric and magnetic vectors of the reflected and transmitted waves [see Eqs. (4) and (6)]. Here we limit ourselves to calculation of the absorption coefficient A of the system under consideration. For this, we use the relation $A = 1 - (R + T)$ where R and T are the reflection and transmission coefficients, respectively, defined as

$$R = \left|\mathrm{Re}(\mathbf{E}_r \times \mathbf{H}_r^*)\right| / \left|\mathrm{Re}(\mathbf{E}_i \times \mathbf{H}_i^*)\right|,$$
$$T = \left|\mathrm{Re}(\mathbf{E}_t \times \mathbf{H}_t^*)\right| / \left|\mathrm{Re}(\mathbf{E}_i \times \mathbf{H}_i^*)\right|. \quad (15)$$

For numerical calculations we take into account that components of the LC dielectric tensor are connected with the components of the LC director by expression $\varepsilon_{1ij} = n_o^2\delta_{ij} + (n_e^2 - n_o^2)\, n_i n_j$, where n_i denotes the components of the director $\boldsymbol{n} = (\sin\psi,\ 0,\ \cos\psi)$. Here ψ is the director angle with the z-axis (see Fig. 1), n_o and n_e are the refractive indices of the ordinary and extraordinary waves, respectively,[29] $i = x, y, z$. As an example of the LC we take the nematic LC W1791 with $n_o \approx 1.53$, $n_e \approx 1.94$ at $\lambda = 1.064\ \mu m$ studied in Ref. 30 and used by us in the case of the graphene grating.[18] It will be convenient for comparison with the corresponding results obtained for the graphene grating. The refractive indices of W1791, n_o and n_e, are not known in far-infrared spectral range. For this range we use the extended Cauchy dispersion formulas obtained in Ref. 31 for the LC E7. Such extrapolation into sufficiently remote spectral region can give a substantial error and in this case the obtained numerical values must be considered as an estimation. As an example of the isotropic substrate material, silicon was chosen as it is often used in graphene plasmonics ($\varepsilon_2 = 11.7$).[32]

III. RESULTS OF CALCULATIONS AND DISCUSSION

A. MoS_2 micro-ribbon grating

The absorption spectra of the MoS_2 micro-ribbon grating placed between a nematic LC and an isotropic dielectric substrate is studied, as is the influence on these spectra of the LC director orientation. In this case, in Fig. 1 conductivity σ_1 refers to MoS_2, $\sigma_2 = 0$, and d is the MoS_2 ribbon width.

We treat here MoS_2 as a monolayer film like graphene. In the infrared and terahertz spectral regions, the intraband contribution to the MoS_2 conductivity dominates.[24] The 2D conductivity of n-doped monolayer MoS_2 can be written in the Drude form as[14,24]

$$\sigma_{MoS2} = \frac{n_{2D}\, e^2}{m_e^*} \frac{\tau_{MoS2}\, i}{\omega\, \tau_{MoS2} + i}, \quad (16)$$

where n_{2D} is the 2D electron concentration of MoS_2, τ_{MoS2} is the electron relaxation time, and m_e^* is the electron effective mass. For monolayer MoS_2 we use the values $\tau_{MoS2} = 0.17$ ps and $m_e^* = 0.53\, m_e$[24] where m_e is the mass of electron.

Figure 2 shows the dependence of absorption spectra of the MoS_2 micro-ribbon grating on the 2D electron concentration in the MoS_2 ribbon. The grating spacing value is fixed and equal to

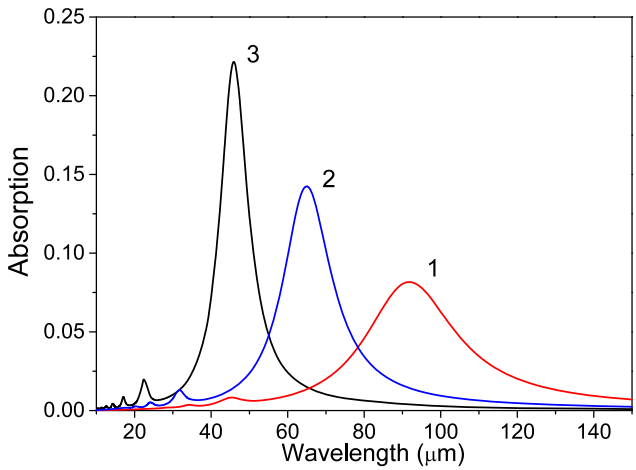

FIG. 2. Absorption spectra of the MoS_2 micro-ribbon grating at different 2D electron concentrations: (1) $n_{2D} = 2.5 \times 10^{13}\,cm^{-2}$, (2) $5 \times 10^{13}\ cm^{-2}$, (3) $10^{14}\ cm^{-2}$. Grating spacing of $\Lambda = 1\ \mu m$, the ribbon aspect ratio $d/\Lambda = 0.5$, the director angle $\psi = 0°$.

$\Lambda = 1$ μm, ribbon aspect ratio $d/\Lambda = 0.5$, and the director angle $\psi = 0°$. Maxima in absorption spectra correspond to the excitation of the plasmon modes in the MoS_2 micro-ribbons. As one can see, the plasmon resonance wavelength shifts with an increase of electron concentration into the short-wavelength side that correlates with a corresponding increase of the plasmon frequency. The magnitude of absorption maxima also increases.

Figure 3 illustrates the change of the absorption spectra of the MoS_2 micro-ribbon grating at the change of the LC director orientation from the homeotropic orientation near the grating ($\psi = 0°$) to the planar one ($\psi = 90°$) for several values of the ribbon width to grating spacing ratio: $d/\Lambda = 0.3$, 0.5 and 0.7. The grating spacing value was fixed and equal to $\Lambda = 1$ μm (Fig. 3a) and $\Lambda = 0.1$ μm (Fig. 3b).

As we can see from Figs. 3a and 3b, a decrease of the grating spacing from $\Lambda = 1$ μm to $\Lambda = 0.1$ μm shifts the resonance peaks into the short-wavelength side. At a fixed grating spacing Λ, an increase of the ribbon width leads to the resonance peak shift into the long-wavelength side and an increase of the resonance peak magnitude. It should also be noted that the magnitude of each peak at the fixed value of ratio d/Λ is the same for different values of the grating spacing Λ. This behavior of the MoS_2 grating plasmon peaks agrees with the results obtained in papers[18,33] for the graphene grating. In particular, following from the qualitative theory developed in Ref. 33 dependence of the resonance wavelength on the ribbon width, $\lambda_r \sim d$, agrees well with data presented in Figs. 3a and 3b.

Magnitudes of maxima in Fig. 3 depend on the LC director orientation. The rotation of the LC director by 90° leads to the change of the maxima magnitude by approximately 9.4-11.9% in Fig. 3a and 9.9-11% in Fig. 3b. The impact of the director rotation on the absorption peak magnitude is more significant for a greater aspect ratio d/Λ.

Note that our results are obtained assuming that the plasmon bands fall into the transparency region of the LC. If the LC absorption bands are not very wide, one can shift the plasmon bands into the LC transparency region choosing the corresponding value of the MoS_2 grating spacing, the ribbon width, and the isotropic substrate material.

B. Graphene-MoS_2 micro-ribbon grating

In this subsection, the features of the absorption spectra of the grating comprised of alternating ribbons of MoS_2 and graphene placed between a nematic LC and an isotropic dielectric substrate is discussed. In this case, we set conductivities σ_1 and σ_2 (see Fig. 1) relating to graphene and MoS_2, respectively, with d to be the graphene ribbon width, $\Lambda - d$ to be the MoS_2 ribbon width, and σ_2 defined by Eq. (16).

The 2D conductivity of graphene in the infrared and terahertz spectral regions can be written as[2]

$$\sigma_{graphene} = \frac{e^2 E_F}{\pi \hbar^2} \frac{\tau_G\, i}{\omega \tau_G + i}, \tag{17}$$

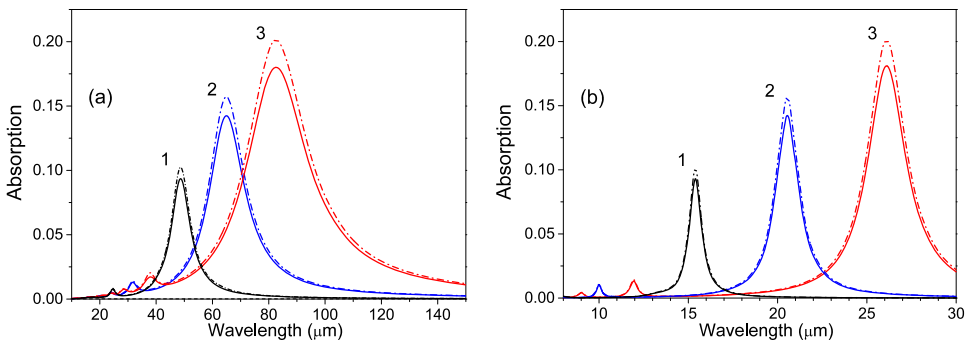

FIG. 3. Absorption spectra of the MoS_2 micro-ribbon grating at different angles of the nematic director and for different values of the ribbon aspect ratio d/Λ at fixed grating spacing. Grating spacing $\Lambda = 1$ μm - (a), $\Lambda = 0.1$ μm - (b). $\psi = 0°$ - solid line, $\psi = 90°$ - dot-dashed line. Ratio $d/\Lambda = 0.3$ - curves 1, $d/\Lambda = 0.5$ - curves 2, $d/\Lambda = 0.7$ - curves 3. 2D electron concentration $n_{2D} = 5 \times 10^{13}\text{cm}^{-2}$.

where E_F is the Fermi energy of graphene, τ_G is the electron relaxation time, and e is the electron charge. For evaluation of the electron relaxation time we use the formula $\tau_G = \mu E_F/(ev_F^2)$, where μ is the carrier mobility, $v_F = 3 \times 10^6$m/s is the Fermi velocity in graphene.[2] Setting $E_F = 0.64$ eV and the carrier mobility $\mu = 0.5$ m^2/(V·s),[2,33] the electron relaxation time $\tau_G = 0.32$ ps is obtained.

In Figs. 4–6 results of our numerical calculations of absorption spectra of the graphene-MoS_2 micro-grating for various grating parameters are presented. In Figs. 4 and 5 we show the influence of the 2D electron concentration in the MoS_2 ribbons on the absorption spectra at two values of the ribbon width to grating spacing ratio $d/\Lambda = 0.5$ (Fig. 4) and $d/\Lambda = 0.7$ (Fig. 5) setting the grating spacing to be fixed and equal to $\Lambda = 1$ μm.

As seen from Fig. 4a, the wavelength of the main peak (~37 μm) in the absorption spectra of the graphene-MoS_2 grating at the MoS_2 ribbon electron concentration $n_{2D} = 10^{13}$cm^{-2} coincides closely with the wavelength of absorption peak of the graphene grating (see Ref. 18). Referring to the results shown in Fig. 2, an absorption in the MoS_2 micro-ribbon grating can appear only at wavelengths much greater than 37 μm for this electron concentration. The influence of this MoS_2 ribbon electron concentration is therefore small and the main absorption peak in Fig. 4a arises mainly due to the plasmon resonance in the graphene micro-ribbons. At $n_{2D} = 2.5 \times 10^{13}$cm^{-2}, the absorption spectrum changes significantly (see Fig. 4b) and three absorption peaks of the plasmon modes are observed instead of the main peak at $n_{2D} = 10^{13}$cm^{-2}. Further increasing n_{2D} (see Figs. 4c and 4d), the resonance wavelengths of the plasmon modes shift toward shorter wavelengths, the magnitude of the absorption peaks decreases, and the plasmon mode with the smallest absorption peak disappears. As in the case of the MoS_2 grating, the shorter wavelength shift of the plasmon modes in the graphene-MoS_2 grating correlates with corresponding increase of the plasmon frequency. At the same time, a decrease and disappearance of the peaks take place because the conductivity of the graphene and MoS_2 micro-ribbons equalizes with an increase of the MoS_2 ribbon electron concentration leading to a decrease of the refractive index grating magnitude.

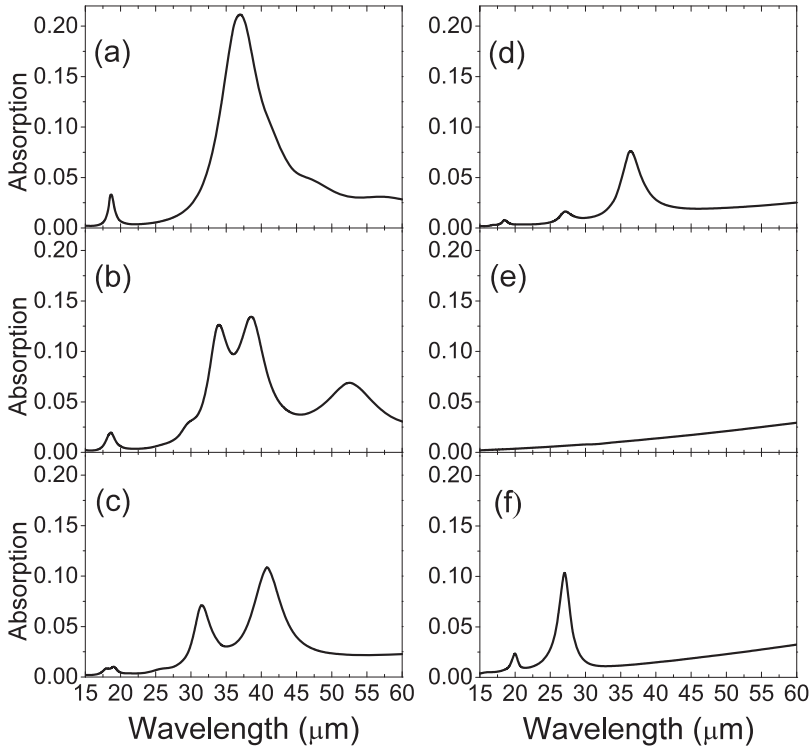

FIG. 4. Absorption spectra of the graphene-MoS_2 micro-ribbon gratings at different 2D electron concentrations: n_{2D} (in cm^{-2}) = 10^{13} - (a), 2.5×10^{13} - (b), 5×10^{13} - (c), 7.7×10^{13} - (d), 14.4×10^{13} - (e), 25×10^{13} - (f). Grating spacing $\Lambda = 1$ μm, aspect ratio $d/\Lambda = 0.5$, director angle $\psi = 0°$.

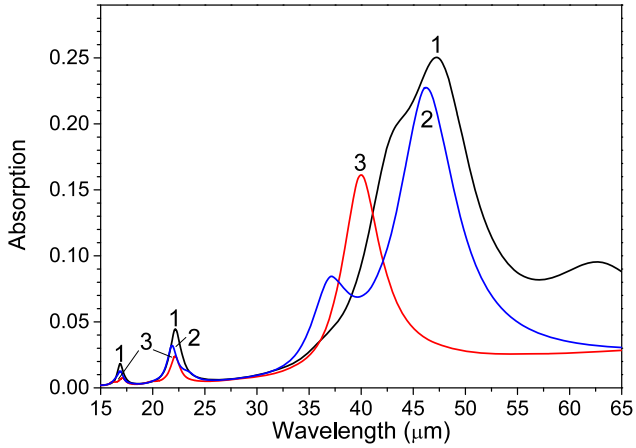

FIG. 5. Absorption spectra of the graphene-MoS_2 micro-ribbon gratings at different 2D electron concentrations: n_{2D} (in cm^{-2}) = (1) 10^{13}, (2) 2.5×10^{13}, (3) 5×10^{13}. Grating spacing $\Lambda = 1$ μm, aspect ratio $d/\Lambda = 0.7$, director angle $\psi = 0°$.

At $n_{2D} = 14.4 \times 10^{13}cm^{-2}$, Im σ_1 = Im σ_2 per calculations. In this case, the refractive index grating as such disappears, plasmons cannot be excited and no plasmon peaks in absorption spectrum of the graphene-MoS_2 structure (Fig. 4e) are observed. The plasmon mode absorption peaks reappear in the shorter wavelength part of absorption spectrum when Im σ_2 > Im σ_1. Fig. 4f shows the case for $n_{2D} > 14.4 \times 10^{13}cm^{-2}$.

With an increasing share of graphene on the grating period ($d/\Lambda = 0.7$), the position of the main resonance peaks in the absorption spectrum shifts towards longer wavelengths (Fig. 5) in comparison with the case $d/\Lambda = 0.5$ (Fig. 4). This is similar to the graphene and MoS_2 gratings case. For this wavelength region the influence of the MoS_2 ribbon electron concentration on the absorption spectrum is more pronounced even at small values of $n_{2D} = 10^{13}cm^{-2}$ (compare Fig. 4a and Fig. 5, curve 1). With an increase of n_{2D}, as in the case of $d/\Lambda = 0.5$, absorption peaks shift toward shorter wavelengths and their magnitude decreases. The smallest absorption peaks disappear, but it takes place at smaller concentrations n_{2D} than in the case $d/\Lambda = 0.5$ (Fig. 5, curves 2 and 3).

In Fig. 6 we show results of calculations of the graphene-MoS_2 micro-grating absorption spectra for two limiting values of the LC director angle at $\psi = 0°$ and $\psi = 90°$ for the graphene ribbon width to grating spacing ratio $d/\Lambda = 0.3$, 0.5 and 0.7. The electron concentration in the MoS_2 ribbons is fixed and equal to $n_{2D} = 5 \times 10^{13}cm^{-2}$, and the grating spacing Λ equals 1 μm in Fig. 6a and 0.1 μm in Fig. 6b.

In Fig. 6a,b the absorption peaks which correspond to the different plasmon modes at a fixed electron concentration in the MoS_2 ribbons are shown. The magnitude and spectral position λ_r of the

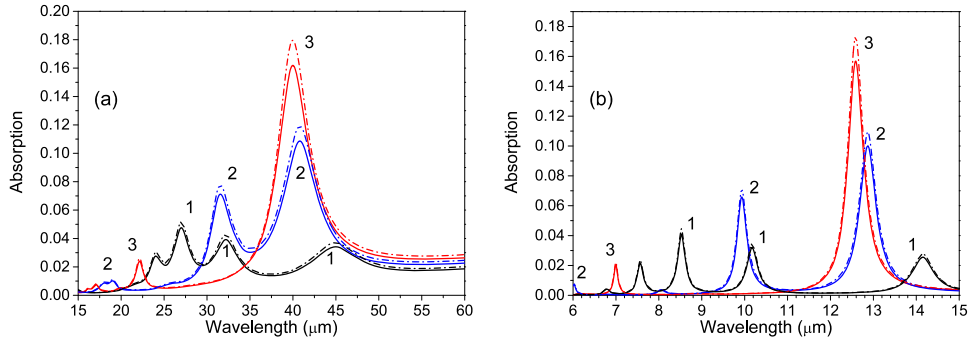

FIG. 6. Absorption spectra of the graphene-MoS_2 micro-ribbon grating at different values of the LC director angle ψ and different aspect ratios d/Λ at fixed grating spacing. Grating spacing (a) $\Lambda = 1$ μm, (b) 0.1 μm. $\psi = 0°$ - solid line, $\psi = 90°$ - dot-dashed line. Ratio $d/\Lambda = 0.3$ - curves 1, $d/\Lambda = 0.5$ - curves 2, $d/\Lambda = 0.7$ - curves 3. Concentration $n_{2D} = 5 \times 10^{13}cm^{-2}$.

plasmon peaks depend on the grating spacing and the ribbon width. As in the case of the graphene and MoS_2 gratings, values of λ_r decrease with a decrease of the grating spacing. However, the character of the λ_r dependence on the ribbon width still depends on the MoS_2 ribbon electron concentration n_{2D}. Figure 6 shows that at $n_{2D} = 5 \times 10^{13}cm^{-2}$, values of λ_r decrease with increasing graphene ribbon width while for smaller MoS_2 ribbon electron concentration ($n_{2D} = 10^{13}cm^{-2}$), this dependence becomes opposite (compare Fig. 4a and Fig. 5, curve 1). To explain this, additional study of gratings with different types of the micro-ribbon materials is needed.

The most intensive plasmon mode absorption peaks are in the spectral range 35-45 μm for $\Lambda = 1$ μm (Fig. 6a) and 11.6-13.6 μm for $\Lambda = 0.1$ μm (Fig. 6b). Reorientation of the LC director from homeotropic orientation ($\psi = 0°$) to planar orientation ($\psi = 90°$) influences only the magnitude of absorption peaks. In particular, the rotation of the LC director by $\psi = 90°$ leads to a change of the absorption peak magnitude by approximately 5.7- 10.8% in the spectral range 35-45 μm (Fig. 6a) and 8.6-10.7% in the spectral range 11.6-13.6 μm (Fig. 6b). Influence of the director rotation on the absorption peak magnitude increases with the aspect ratio of the ribbon material, which dominates the conductivity, i.e. the ratio d/Λ in the cases presented in Figs. 6a and 6b. This is due to the corresponding increase of the refractive index grating magnitude and agrees with results obtained for graphene[18] and MoS_2 gratings.

IV. CONCLUSIONS

The absorption spectra of MoS_2 and graphene-MoS_2 micro-ribbon gratings placed between a nematic LC and isotropic dielectric media was studied theoretically. In the far-infrared region (6-140 μm) maxima in the absorption spectra related to the excitation of plasmons within the micro-ribbons are observed. For fixed parameters of the micro-ribbon conductivity, the spectral position of absorption maxima depends on the grating spacing and micro-ribbon width. The influence of the 2D electron concentration of the MoS_2 ribbons, n_{2D}, on the absorption spectra was explored and is shown to be different for the MoS_2 and the graphene-MoS_2 grating cases. For the MoS_2 grating case, a shift of the absorption peaks toward shorter wavelengths and an increase of their magnitude with increasing n_{2D} was observed. For the graphene-MoS_2 grating case, an increase of n_{2D} leads first to the appearance of new plasmon modes and a shift of their absorption peaks to shorter wavelengths, and then a gradual decrease of the peak magnitude (to include some mode disappearance). This occurs because the conductivities of MoS_2 and graphene ribbons equalize with increase n_{2D} resulting in a decrease of the refractive index grating magnitude. When the imaginary parts of the MoS_2 and graphene ribbon conductivity are equal, the refractive index grating disappears, and all plasmon peaks disappear. Upon further increasing of n_{2D} the absorption peaks appear again in the shorter wavelength part of the spectrum. The spectral shift of absorption maxima dependence on the ribbon width can be on the short- or long-wavelength side depending on n_{2D}.

We show that the magnitude of absorption peaks in the MoS_2 and the graphene-MoS_2 gratings depends on the LC orientation state. The results indicate manipulation of the absorption maximum value within 10-12% of its magnitude using this change. The influence of the LC orientation state change on the plasmonic resonance increases with an increase of the MoS_2 ribbon width to grating spacing ratio for the MoS_2 grating, and the graphene ribbon width to grating spacing ratio for the graphene-MoS_2 grating. Our results can be used for designing new types of photonic structures coupling the dynamic properties of LC molecules with baseline plasmonic properties of MoS_2 and the graphene-MoS_2 gratings.

ACKNOWLEDGMENTS

This work was partially supported by EOARD Grant 15IOE011.

[1] L. Ju, B. Geng, J. Horng, C. Girit, M. Martin, Z. Hao, H. A. Bechtel, X. Liang, A. Zettl, Y. R. Shen, and F. Wang, Nat. Nanotech. **6**, 630 (2011).
[2] W. Gao, J. Shu, C. Qiu, and Q. Xu, ACS Nano **6**, 7806 (2012).
[3] H. Yan, T. Low, W. Zhu, Y. Wu, M. Freitag, X. Li, F. Guinea, P. Avouris, and F. Xia, Nat. Photonics **7**, 394 (2013).
[4] Y.-Q. Liu and P.-K. Liu, J. Appl. Phys. **121**, 113104 (2017).
[5] A. Ferreira and N. M. R. Peres, Phys. Rev. B **86**, 205401 (2012).

[6] T. M. Slipchenko, M. L. Nesterov, L. Martin-Moreno, and A. Yu. Nikitin, J. Opt. **15**, 114008 (2013).
[7] R. Alaee, M. Farhat, C. Rockstuhl, and F. Lederer, Opt. Express **20**, 28017 (2012).
[8] Y.-L. Xu, E.-P. Li, X.-C. Wei, and D. Yi, IEEE Microw. Wirel. Compon. Lett. **26**, 10 (2016).
[9] S. Ke, B. Wang, H. Huang, H. Long, K. Wang, and P. Lu, Opt. Express **23**, 8888 (2015).
[10] Z. H. Zhu, C. C. Guo, K. Liu, J. F. Zhang, W. M. Ye, X. D. Yuan, and S. Q. Qin, J. Appl. Phys. **116**, 104304 (2014).
[11] Y. M. Xiao, W. Xu, B. Van Duppen, and F. M. Peeters, Phys. Rev. B **94**, 155432 (2016).
[12] C. J. Docherty, P. Parkinson, H. J. Joyce, M.-H. Chiu, C.-H. Chen, M.-Y. Lee, L.-J. Li, L. M. Herz, and M. B. Johnston, ACS Nano **8**, 11147 (2014).
[13] X. Yan, L. Zhu, Y. Zhou, Y. E, L. Wang, and X. Xu, Appl. Opt. **54**, 6732 (2015).
[14] J. H. Buss, R. P. Smith, G. Coslovich, and R. A. Kaindl, Proc. of SPIE **9361**, 93611J (2015).
[15] A. Kasry, M. A. Kuroda, G. J. Martyna, G. S. Tulevski, and A. A. Bol, ACS Nano **4**, 3839 (2010).
[16] K. S. Novoselov, A. K. Geim, S. V. Morozov, D. Jiang, Y. Zhang, S. V. Dubonos, I. V. Grigorieva, and A. A. Firsov, Science **306**, 666 (2004).
[17] J. Kim, H. Son, D. J. Cho, B. Geng, W. Regan, S. Shi, K. Kim, A. Zettl, Y.-R. Shen, and F. Wang, Nano Lett. **12**, 5598 (2012).
[18] V. Yu. Reshetnyak, V. I. Zadorozhnii, I. P. Pinkevych, and D. R. Evans, Phys. Rev. E **96**, 022703 (2017).
[19] G. Si, Y. Zhao, E. S. P. Leong, and Y. J. Liu, Materials **7**, 1296 (2014).
[20] A. Scholz, T. Stauber, and J. Schliemann, Phys. Rev. B **88**, 035135 (2013).
[21] T. Low, A. Chaves, J. D. Caldwell, A. Kumar, N. X. Fang, P. Avouris, T. F. Heinz, F. Guinea, L. Martin-Moreno, and F. Koppens, Nature Materials **16**, 182 (2017).
[22] B. Radisavljevic and A. Kis, Nature Materials **12**, 815 (2013).
[23] W. Zheng, F. Fan, M. Chen, S. Chen, and S.-J. Chang, AIP Advances **6**, 075105 (2016).
[24] S. Chen, F. Fan, Y. Miao, X. He, K. Zhang, and S. Chang, Nanoscale **8**, 4713 (2016).
[25] Y. Shi, W. Zhou, A.-Y. Lu, W. Fang, Y.-H. Lee, A. L. Hsu, S. M. Kim, K. K. Kim, H. Y. Yang, L.-J. Li, J.-C. Idrobo, and J. Kong, Nano Lett. **12**, 2784 (2012).
[26] Y.-C. Lin, N. Lu, N. Perea-Lopez, J. Li, Z. Lin, X. Peng, C. H. Lee, C. Sun, L. Calderin, P. N. Browning, M. S. Bresnehan, M. J. Kim, T. S. Mayer, M. Terrones, and J. A. Robinson, ACS Nano **8**, 3715 (2014).
[27] M. Zhao, Y. Ye, Y. Han, Y. Xia, H. Zhu, S. Wang, Y. Wang, D. A. Muller, and X. Zhang, Nat. Nanotech. **11**, 954 (2016).
[28] X. Ling, Y. Lin, Q. Ma, Z. Wang, Y. Song, L. Yu, S. Huang, W. Fang, X. Zhang, A. L. Hsu, Y. Bie, Y.-H. Lee, Y. Zhu, L. Wu, J. Li, P. Jarillo-Herrero, M. Dresselhaus, T. Palacios, and J. Kong, Adv. Mater. **28**, 2322 (2016).
[29] P. G. de Gennes and J. Prost, *The Physics of Liquid Crystals*, 2nd ed. (Oxford University Press, Oxford, 1995).
[30] E. Nowinowski-Kruszelnicki, J. Kędzierski, Z. Raszewski, L. Jaroszewicz, R. Dąbrowski, M. Kojdecki, W. Piecek, P. Perkowski, K. Garbat, M. Olifierczuk, M. Sutkowski, K. Ogrodnik, P. Morawiak, and E. Miszczyk, Optica Applicata **42**, 167 (2012).
[31] J. Li, S. T. Wu, S. Brugioni, R. Meucci, and S. Faetti, J. Appl. Phys. **97**, 073501 (2005).
[32] J. Dai, J. Zhang, W. Zhang, and D. Grischkowsky, J. Opt. Soc. Am. B **21**, 1379 (2004).
[33] A. Yu. Nikitin, F. Guinea, F. J. Garcia-Vidal, and L. Martin-Moreno, Phys. Rev. B **85**, 081405 (2012).